Highlighting research from R. Morris *et al.* at the Soft Matter group, University of Leeds.

Variable pitch hydrodynamic electro-optic gratings utilising bent liquid crystal dimers

Liquid crystal electrohydrodynamic instabilities as diffractive structures. Liquid crystals when subjected to external electric field may form continuously variable diffractive structures. We test the influence of material and device parameters on these structures and the potential for continuous beam steering of light.

As featured in:

See M. Nagaraj *et al.*,
Soft Matter, 2020, **16**, 10439.

ROYAL SOCIETY
OF **CHEMISTRY**

rsc.li/soft-matter-journal

Check for updates

Variable pitch hydrodynamic electro-optic gratings utilising bent liquid crystal dimers†

R. Morris, [ID] J. C. Jones [ID] and M. Nagaraj [ID] *

Electrohydrodynamic instabilities (EHDI) in liquid crystals form uniform and continuously variable diffractive structures when subject to certain material and geometry determined conditions. A one-dimensional grating is one such diffractive structure, where the refractive index changes periodically in a direction parallel to the initial liquid crystal director. The period of this structure has been shown previously to vary continuously between the values of the cell gap and half-cell gap approximately, allowing continuous angular modulation of optical beams but with a limited angular range. In this work, the lower pitch limit is shown to also be governed in part by the ratio of the splay and bend elastic constants (k_{11}/k_{33}) of the liquid crystal. A host nematic liquid crystal with standard elastic constant ratios ($k_{11}/k_{33} < 1$) is doped with odd-alkyl-spaced dimeric liquid crystal CB7CB, to create a liquid crystal mixture with a far higher elastic constant ratio ($k_{11}/k_{33} > 5$) than for those previously used in literature EHDI studies. The EHDI gratings formed in this new mixture exhibit pitch lengths significantly below half-cell gap, allowing up to 50% wider angle continuous steering of light. This improves the potential for application in beamsteering and diffractive optical devices.

Introduction

Since the 1960s nematic liquid crystals (NLCs) have been used successfully as switchable optical materials in optoelectronic applications, including displays.[1,2] The number of different applications of NLCs has expanded in recent decades to a wider variety of optical devices including spatial light modulators,[3–8] lenses,[9–11] diffraction gratings[12–15] and beamsteering devices.[4,16–18] An important goal has been to produce entirely arbitrary phase profiles for incident light when passed through the liquid crystal. Currently, liquid crystal on silicon (LCoS) spatial light modulators are used for such purposes.[3–8,19–22] In LCoS devices, individual electrodes, driven by the silicon back-plane, reorient the NLC to induce the required optical phase profile. However, fringing fields and defects in the nematic director profile limit pixels to a minimum size of ~ 5 μm.[8,16] Given that many pixels are required to create all but the simplest optical features, and the fact that LCoS devices operate in reflection mode only (with much larger minimum pixel sizes for transmissive devices),[5,16] developing alternative methodologies to create high-quality diffractive structures is desirable. In most NLC devices the electro-optic switching is achieved by utilising an external electric field, in order to rotate the average molecular orientation (**n**, the director), and hence the optic axis (Fréedericksz transition).[23,24] The required electric field is mainly dictated by the dielectric anisotropy ($\Delta\varepsilon$) and the elastic constants for splay (k_{11}), twist (k_{22}) and bend (k_{33}),[24–26] of the NLC. Optimisation of these material parameters is an essential part of ensuring good device performance.

A less conventional method for creating diffractive optical structures in NLCs is by inducing viscous flow. Here, director reorientation is achieved by inducing a periodic material flow, which places a viscous torque on the director, causing it to reorient and form an optical grating.[27,28] An example of such a process is the formation of electrically driven ion flow patterns created by electrohydrodynamic instability (EHDI).

In EHDIs the periodicity, described by pitch length (λ_C) of the induced optical grating, is typically dictated by the device spacing, d, the conductivity anisotropy ($\Delta\sigma$) and the dielectric anisotropy ($\Delta\varepsilon$). The material elastic constants play a key role, as for the grating to form the systems elastic inertia must be overcome.[28–30] In our previous work,[31] it was argued that, for a given d, k_{11} and k_{33} influence the aspect ratio and the pitch length of the EHDI rolls, respectively. In this paper, the effect of changing the values of k_{11} and k_{33} of the NLC on the resulting EHDI is investigated by comparing different materials in several devices of different spacing. The variation in material elasticity is achieved by adding an odd-spaced dimer to the NLC. This increases k_{11}/k_{33} to an atypical level, which is confirmed through

School of Physics and Astronomy, University of Leeds, Leeds LS2 9JT, UK.
E-mail: m.nagaraj@leeds.ac.uk

† Electronic supplementary information (ESI) available. See DOI: 10.1039/d0sm01425g

the measurements of elastic constants. This results in shorter pitch EHDI gratings (<half-cell gap) than observed previously, thereby allowing wider angle continuous beamsteering steering.

Electro-hydro-dynamic instabilities

EHDIs have been the focus of extensive study since Williams first observed them in 1963. Such Williams domains are periodic structures that form when a relatively low-frequency voltage is applied across a layer of NLC.[32,33] These periodic domains are formed by the reorientation of the NLC's optic axis, resulting in a periodic change of the refractive index for light polarised parallel to the axis of the grating vector. This change can be observed using both polarising optical microscopy (POM)[32,34,35] and diffraction spectroscopy.[15,27–29,36–38]

A basic understanding of the induced periodic domains was provided by Carr[39] and Helfrich[40] using a one-dimensional model based on periodic viscous flow and charge separation, leading to the standard model of EHDIs still used.[27–30,34,36,41–45]
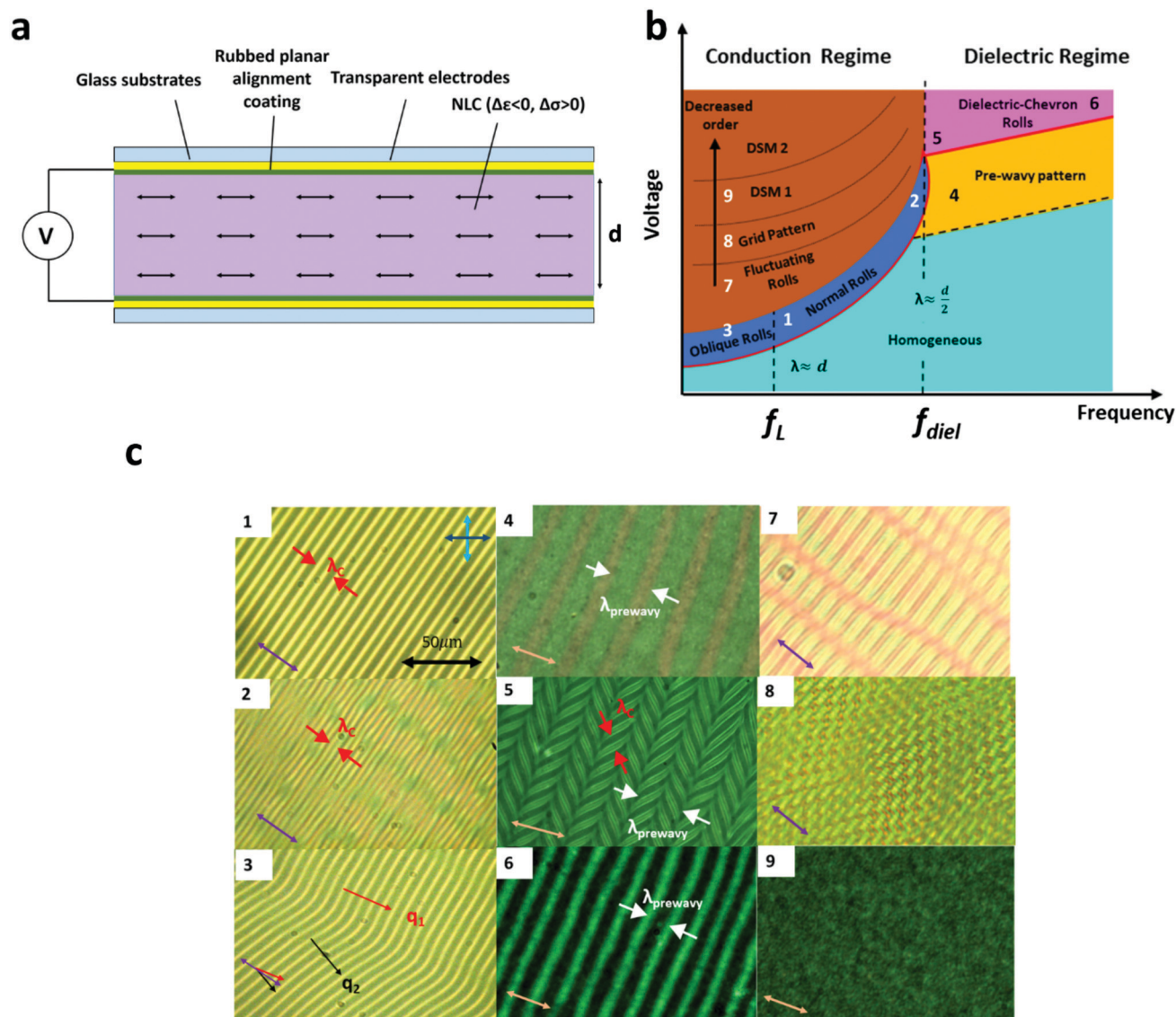

Fig. 1 (a) Schematic representation of a device that can undergo EHDI. A thin layer of nematic liquid crystal with negative $\Delta\varepsilon$ and positive $\Delta\sigma$ is placed between two glass plates separated by spacing d. The glass is coated with a transparent conductor, which allows a voltage V to be applied across the material, and an alignment layer, which gives the director (represented by double-headed arrows) an initial orientation. (b) Plot of the textures usually observed in standard EHDI as a mapping of voltage and frequency (see ref. 28). Here the threshold/critical voltage (V_C) for onset of EHDI is shown as the red line below which the texture is homogenous. This behaviour of V_C consists of the low frequency 'conduction' and high frequency 'dielectric' regimes. The focus of this work is the narrow region above V_C in the conduction regime where well ordered normal rolls exist. (c) POM images of different regions shown in (b) between crossed polarisers where the scale bar in 1 applies to all figures. Here the rubbing direction is shown as either the pink or purple double headed arrow in the bottom left of each Fig. 1 and 2 shows the Normal Roll (NR) mode. 3 shows oblique rolls which occur at lower frequencies and have two wave vectors q_1 and q_2 oriented at $\pm\theta_{Ob}$ to the rubbing direction respectively. 4–6 show prewavy patterns. Here 5 shows a chevron texture, which is formed by the superposition of the NR and prewavy instabilities[51,53] 7–9 show the effect of increasing voltage within the conductive regime, where temporal and spatial disorder increases until the Dynamic Scattering Modes (DSM's 1 and 2) happen. DSMs are highly efficient optical scattering states.

This standard model is most straightforward for materials with negative dielectric ($\Delta\varepsilon < 0$) and positive conductivity ($\Delta\sigma > 0$) anisotropies operating in a planar-aligned device, as shown schematically in Fig. 1a. Here, domain formation occurs once the applied voltage, V reaches a critical value, V_C. This threshold is expected to vary with frequency in the manner shown in Fig. 1b, where two distinct regimes, 'conduction' and 'dielectric', are observed.[27,28,41,44,46,47] In this work, we focus on the lower frequency conduction regime. In the conduction regime at V_C, a one-dimensional phase contrast grating forms, with normal parallel to the initial director (Fig. 1c). Within this normal roll (NR) mode, the period (λ_C) decreases with increasing applied frequency.[31,46]

When V_C is applied, the NR mode is induced by periodic hydrodynamic domains within the material (Fig. 2a). These domains are caused by ions moving to oppositely charge electrodes while the voltage oscillates. This has the dual effect of applying a viscous torque on the director[29,48] and inducing a periodic charge separation in the material creating an in-plane electric field (shown as E_{ions} in Fig. 2b). Both the hydrodynamic motion and the in-plane potential act to deviate the director inside the roll from its initial orientation. The resulting out-of-plane disruption of the director is resisted by the applied voltage across the device (due to negative $\Delta\varepsilon$) and the material elasticity.[28,29,39,40,45,49] This accounts for the threshold behaviour

of V_C, where for a given frequency, the combined deforming torques overcome the system inertia allowing the director within the rolls reorient when $V > V_C$. At V_C, this creates a NR mode phase modulating diffraction grating of the same period as the director modulation.[15,37] The value of V_C is seen to increase with applied frequency (Fig. 1a), as ions have shorter time periods to transit the cell.

At the onset of NR mode, the bend elastic constant, k_{33} is the dominant elasticity that must be overcome for the initial deviation of the director to occur.[28,29] Meanwhile, the value of k_{11} becomes important at higher deviation. This is analogous to the Fréedericksz transition of a negative $\Delta\varepsilon$ material with the field applied parallel to the initial director. As mentioned previously, this suggests that a low k_{33} (and hence high ratio of k_{11}/k_{33}) should be advantageous for low pitch high contrast diffraction gratings: larger k_{11} implies any deformation will persist further in the z-direction, while a low k_{33} implies shorter pitch rolls (λ_C decreases).[31]

While maintaining the uniform NR mode, the range of pitches (λ_C) the rolls can exhibit is typically dictated by the device spacing, d. Here, the pitch only occupies values in the approximate range[31,35,37,50–52]

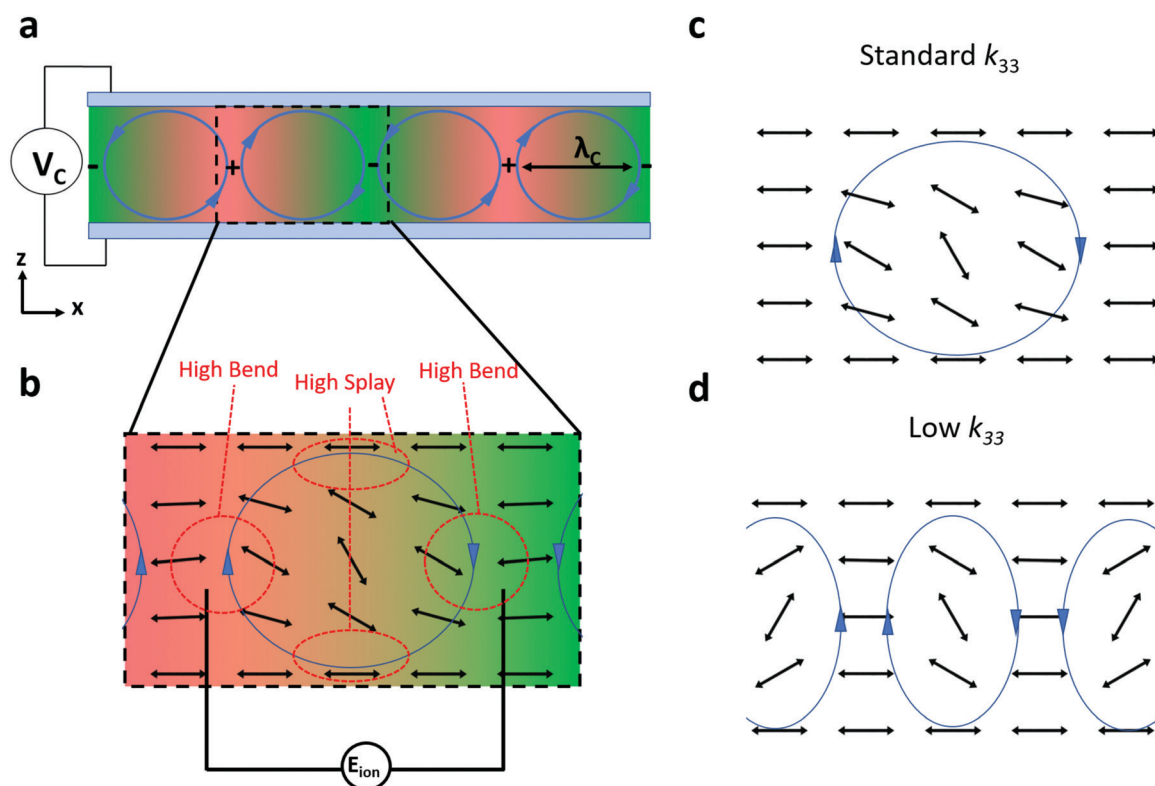$$\frac{d}{2} \leq \lambda_C \leq d, \tag{1}$$

Fig. 2 EHDI in the conduction regime, with a focus on the role of elastic constants in determining the grating size. (a) Schematic of typical roll formation in a device such as that shown in Fig. 1a when V_C is applied. The hydrodynamic rolls are represented by the circles, with arrows showing the direction of flow. (b) Schematic of the director configuration within a roll, where the director rotates due to the combined effects of the viscous torque and periodic charge separation, represented by the electric field, E_{ions}. (c) and (d) Schematics of the predicted effect of changing the bend elastic constant on the roll shape,[31] where lower values allow the period of deformation to decrease creating a shorter pitch grating.

before transitioning into the chevron texture (Fig. 1c). Within the NR mode the magnitude of λ_C decreases across this range with increasing frequency. In terms of the wave vector, q_C,

$$q_C = \frac{2\pi}{\lambda_C}, \qquad (2)$$

this range becomes

$$\frac{4\pi}{d} \geq q_C \geq \frac{2\pi}{d}, \qquad (3)$$

or

$$2q_0 \geq q_C \geq q_0, \qquad (4)$$

where q_0 is $2\pi/d$. This severely restricts the range of continuously variable optical diffraction angles[15,29,31,38] that is available when using EHDI. Although reducing the cell gap d does result in higher q_C as desired, there is a concomitant decrease of diffraction efficiency, due to the reduced optical path length of the rolls. To create wider-angle beam steering devices, therefore, other means for decreasing λ_C or increasing q_C are necessary.

EHDI in bent cores and dimers

In recent years, a wealth of novel mesogens have been synthesised, such as bent-core[54–65] and bent dimeric[63,66–80] compounds, which exhibit unusual viscoelasticity, flexoelectricity and phase behaviour. Studies have been carried out in driving bent-core LCs into a state of EHDI[58,61,81–83] and there are a few similar reports on odd-spaced dimeric LCs.[84–86] Both bent-core and dimeric LCs tend to exhibit significantly different EHDI behaviour (termed non-standard electroconvection) to those observed in conventional (calamitic) NLCs.[87–89] These differences are attributed to the sizeable effect of flexoelectricity in the EHDI of these novel materials,[41,83–85] where the standard Carr–Helfrich model assumes such effects are negligible.[34,39,40] The EHDI of bent-core and dimeric LCs show different frequency dependencies of V_C and optical textures, compared to calamitics, making a direct evaluation between standard and non-standard EHDI difficult. In instances where the conductivity is relatively low, low-frequency flexoelectric domains or non-standard rolls appear that are parallel to the director field, contrary to those of standard EHDI.[90,91] Difficulties in comparisons are further compounded as both bent-core and bent dimeric LCs often have nematic phase at elevated temperatures and are usually difficult to align uniformly.

Both bent-core and bent dimeric liquid crystals have been shown to exhibit unusual elastic constants when compared to calamitic NLCs. They exhibit values of k_{11}/k_{33} that are significantly higher than unity,[54,57,60,69,72,76,79,92] where standard calamitics typically exhibit k_{11}/k_{33} between 0.6 and 0.8.[93–95] It has also been shown that doping a standard calamitic liquid crystal with a bent-core or dimeric material can imbue the mixture with some similarly unusual elastic properties[56,92,96–99] while still showing a nematic phase. For example, Parthasarathi et al.[97] showed that binary mixtures of the bent dimer CB7CB with calamitic material 7OCB at certain temperatures exhibits $k_{11}/k_{33} > 5$.

In order to understand the influence of elastic constants on the EHDI formation, our work uses a mixture of a bent dimer (CB7CB) and a standard calamitic NLC (MLC 2081). The permittivities of the resulting mixture were characterised to quantify the changes in dielectric and elastic properties. POM experiments were carried out on the mixture while it underwent EHDI to quantify V_C and q_C. It was hypothesised that if the outlined arguments of large k_{11}/k_{33} are correct, this new mixture should exhibit larger values q_C than those given in eqn (4). Such large values of q_C are beneficial in the goal of achieving wider angle continuous beam steering.

Methods

Materials

Various mixtures of the NLC, MLC 2081, salt, tetra – butyl – ammonium – tetra – phenyl – borate (TBATPB, Fig. 3a) and bent dimer, 1,7-bis(4-cyanobiphenyl-4′-yl)heptane (CB7CB, Fig. 3b) were created. The naming format $M_{MLC:CB7CB:TBATPB}$ is used for convenience, where subscripts represent the weight fraction ratios of MLC 2081, CB7CB and TBATPB respectively. The choice and function of these various components is discussed in the following paragraphs.

MLC 2081 is a commercial NLC mixture provided by Merck Chemicals UK and was chosen as the host liquid crystal because it exhibits a wide nematic temperature range, a typical k_{11}/k_{33} (0.7–0.8 at 25 °C), high negative dielectric anisotropy ($\Delta\varepsilon = -5.5$ at 25 °C) and, importantly, a low inherent conductivity ($\sigma_\perp < 10$ nS m^{-1} at 25 °C) to enable conductivity to be controlled through the addition of dopants. The clearing temperature was measured to be 112 ± 2 °C, (using POM in a 10 μm spaced, planar-aligned glass cell on cooling at 0.5 °C min^{-1}).

Due to its low conductivity and strongly negative $\Delta\varepsilon$, MLC 2081 did not display a typical EHDI conduction regime at frequencies >1 Hz. To enhance it's conductivity, the ionic dopant TBATPB was added in concentrations of 0.5–1.0%
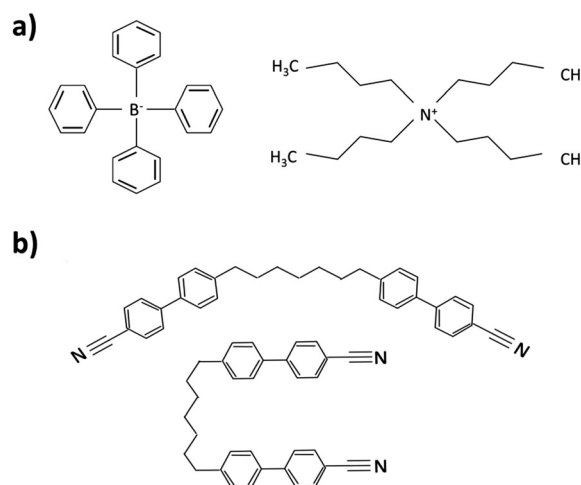

Fig. 3 Chemical structure of (a) TBATPB and (b) CB7CB, shown in the dominant "banana" and "hairpin" conformations.

(creating three mixtures $M_{100:0:0.5/0.6/1.0}$). TBATPB was chosen as it (and other similar salts) has been shown previously to enhance conduction of LCs.[31,56,100,101] Increase of T_{NI} in mixtures were observed when measured over several months and application of high electric fields, potentially due to the breakdown of one of the lower clearing point components in the mixture caused by the addition of the ions. Hence, comparisons are made at the same reduced temperature ($T_{NI} - T$) where T_{NI} was checked at the time of each measurement.

The bent dimeric dopant CB7CB (synthon chemicals) is one of a series of dimers that have received much interest in the past few years as it exhibits a novel nematic phase, called the twist-bend nematic, N_{TB}.[63,66–80] In addition to this, it has been shown that when the dimer is mixed with standard calamitics the resultant mixture can also show N_{TB} phases, as well as exhibit distinctive changes in elastic constants.[96–99] The transitions for the pure CB7CB were measured as Iso 116 °C N 102 °C N_{TB}, in agreement with literature values.[63,67,90] CB7CB has been shown to have a net positive $\Delta\varepsilon$, due to the dominant effect of the longitudinal dipole moment of the "hairpin" conformer over the transverse dipole of the "banana" conformer (Fig. 3b).[70,71] For the EHDI work the mixture composition 60% MLC 2081 and 40% CB7CB ($M_{60:40:0}$) was chosen, since this was the composition with the highest concentration of CB7CB with the desired negative $\Delta\varepsilon$ over a wide nematic range (without the N_{TB} phase). Compared to MLC 2081, $M_{60:40:0}$ showed only a slightly reduced T_{NI} of 102 ± 2 °C and remained nematic until 20 °C. The similar nematic temperature range of the mixture components had the additional advantage that both T and $T_{NI} - T$ could be used for material comparisons. The materials were heated above T_{NI} before any measurements were taken and typically all measurements of a particular type (optical or dielectric) were undertaken in a single cooling cycle. It was noted $M_{60:40:0}$ had sufficiently high conductivity to exhibit a EHDI conduction regime without the addition of TBATPB.

Dielectric studies

The dielectric and elastic properties of the materials were characterised as follows. The mixtures were filled into 10 μm spaced devices with bespoke guarded, circular electrodes for accurate permittivity measurements. We assume that there is no change to the elastic constants caused by the addition of TBATPB due to the low concentrations used. The polyimide SE1211 (Nissan Chemicals) was used to produce homeotropic (HT) alignment (pretilt ~90°), whereas either SE2170 or SE130 (Nissan chemicals) were used for planar homogeneous (PH) alignment, both of which provide low pretilts (~2°).[102] Dielectric studies were performed using an Agilent E4980A LCR meter with coupled Linkam hotstage (TMS 95), to measure device capacitance and conductivity as functions of frequency, voltage and sample temperature. The signal was held at 50 kHz for a period of 60 s before each measurement, which was found to be sufficiently long for the capacitance to settle for all temperatures and voltages. This frequency was also found to be far from any relaxation processes and electrode effects. The measured

capacitance C_m and conductance G_m values for the device includes the effect of the alignment layers. These were converted to measured permittivity components ε_m^* using the 10 kHz empty cell capacitance, C_0:[103]

$$\varepsilon_m' = \frac{C_m}{C_0}; \quad \varepsilon_m'' = \frac{G_m}{\omega C_0}, \tag{5}$$

where ω is the angular frequency of the applied signal. The empty cell measurement frequency was chosen to be as close to that of the filled cell measurements whilst still avoiding electrode effects. As $|\Delta\varepsilon|$ was found to be very small for some of the samples, it was important to account for systematic errors associated with the dielectric contribution of the alignment layers by including two series capacitances in the analysis:

$$C_{AL} = \frac{\varepsilon_0 \varepsilon_{AL} A}{d_{AL}} \tag{6}$$

which gives to a first approximation an adjusted LC permittivity (ε_{LC}) from the measured value of the device

$$\varepsilon_{LC} = \frac{\varepsilon_m}{1 - 2\dfrac{d_{AL}\varepsilon_{LC}}{d_{LC}\varepsilon_{AL}}}, \tag{7}$$

and reduced drop in potential across the LC layer (V_{LC}) compared to that applied to the entire device,

$$V_{LC} = \frac{V}{1 + 2\dfrac{d_{AL}\varepsilon_{LC}}{d_{LC}\varepsilon_{AL}}}. \tag{8}$$

Here, ε_{LC}, d_{LC} and ε_{AL}, d_{AL} are the permitivities and thicknesses of the LC material and alignment layers respectively, and A is the electrode area. The high voltage limit of ε_{LC} was determined using the technique of Clark et al.,[104] and the $\varepsilon_{LC}(V_{LC})$ data was fitted using the method of Welford and Sambles,[105] to give $\varepsilon_\parallel$, $\varepsilon_\perp$, k_{11} and k_{33}. Conductivities were found from frequency scans taken at a fixed voltage of 0.05 V using

$$\sigma = \frac{G_m \cdot d}{A} \tag{9}$$

and a single value σ was taken in the frequency-independent range (typically 1 kHz to 100 kHz, depending on material and temperature). It is assumed in eqn (9) that the alignment layers have sufficiently high resistances to not contribute to conductivity in this frequency range.

Devices

Several devices were used to assess the effects of elastic constants on NR diffraction gratings. These are listed in Table 1. Testing a range of devices allowed the effects of spacing, temperature, conductivity and permittivity on the V_C and q_C values of the NR mode be characterised. In all the devices where an NR mode was observed, the pitch q_C was recorded using POM with a stage micrometer. Each frequency was set, and the applied voltage slowly increased from zero until the instability pattern was visible and the onset voltage V_C

Table 1 Devices used for measurements of V_C and q_C. The table lists the material, spacing, alignment layer used, whether the Normal roll mode EHDI is observed (Y = Yes, N = No) and the T_{NI} at the point of testing. Devices 1 and 2 are pure MLC 2081 with different cell gaps; devices 3–5 have with varying amounts of TBATPB, and devices 6 and 7 have mixtures with 40% bent dimer CB7CB. The polyimides used are all low pretilt (1–2°) ones to simplify device operation

Device	1	2	3	4	5	6	7
Material	$M_{100:0:0}$	$M_{100:0:0}$	$M_{100:0:0.6}$	$M_{100:0:0.5}$	$M_{100:0:1.0}$	$M_{60:40:0}$	$M_{60:40:0}$
Spacing	10.6 ± 0.2	19.6 ± 0.2	10.0 ± 0.2	19.2 ± 0.3	19.1 ± 0.2	10.6 ± 0.4	18.9 ± 0.2
Alignment layer	SE2170	SE130	SE130	SE130	SE130	SE2170	SE130
NR EHDI	N	N	Y	Y	Y	Y	Y
T_{NI} (°C)	112 ± 2	112 ± 2	116 ± 2	129 ± 2^a	115 ± 2	102 ± 2	102 ± 2

^{a} Device 4 has a higher T_{NI} due to the increase in T_{NI} over time and application of field. All other devices were tested immediately on filling.

was found. Within the NR regime, V_C and q_C were described by empirical fits:[31]

$$V_C(f) = V_C(f \to 0)\left(1 + \left(\frac{f}{f_{crit,V}}\right)^4\right) \qquad (10)$$

and

$$q_C(f) = q_C(f \to 0)\left(1 + \left(\frac{f}{f_{crit,q}}\right)^4\right), \qquad (11)$$

where $f_{crit,v}$ and $f_{crit,q}$ are critical frequencies at which the values of V_C and q_C are twice their low-frequency values.

The changes in grating pitch with frequency was confirmed through measurement of the diffraction angles as a function of frequency of the applied field. Results were taken using a HeNe 633 nm laser (Thorlabs) with the polarisation aligned parallel to the x-direction as shown in Fig. 2b, so that the incoming wavefronts experienced the periodic phase modulation. As in previous works,[31,37,38] $m = 2$ gave the highest intensity of the non-zero order diffraction peaks.

Results

Material characterisation

MLC 2081 was found to have a negative $\Delta\varepsilon$ from T_{NI} (measured 112 ± 2 °C) to room temperature. The temperature dependence of the measured $\varepsilon_\perp$, $\varepsilon_\parallel$ and $\bar\varepsilon$ is shown in Fig. 4a, where,

$$\bar\varepsilon = \frac{2\varepsilon_\perp + \varepsilon_\parallel}{3}. \qquad (12)$$

On filling, all samples of MLC 2081 with TBATPB ($M_{100:0:0.5/0.6/1.0}$) had a slightly higher values of T_{NI} in the range 115 ± 3 °C and did not have significantly different measured permittivity values.[31]

The mixture of MLC 2081 and bent dimer CB7CB ($M_{60:40:0}$) had a $T_{NI} = 102 \pm 2$ °C and $\Delta\varepsilon$ which changed sign from weakly positive between 102 °C and 63 °C, to weakly negative below 63 °C. This behaviour is due to the high gradient of permittivities *versus* temperature for the odd dimer mixture, due to the change in distribution of the conformational state from the positive $\Delta\varepsilon$ hairpin conformer to the negative $\Delta\varepsilon$ banana conformer.[66,69,79,80,106] The values of $\varepsilon_\perp$, $\varepsilon_\parallel$ and ε_{iso} of $M_{60:40:0}$ are shown in Fig. 4b, where statistical errors from repeated measurements are used (found to be $\pm 0.5\%$ for $\varepsilon_\perp$, $\varepsilon_\parallel$, 1% for ε_{iso}). To confirm the changing sign of $\Delta\varepsilon$,

the homeotropic (HT) $M_{60:40:0}$ sample was cooled from $T_{NI} + 10$ °C with a 30 V-(10 kHz) voltage continuously applied across the device. Above 63 °C, the sample remained dark since the electric field supported homeotropic alignment where the material has a positive $\Delta\varepsilon$, while below this temperature a Schlieren texture was observed, due to the material undergoing a Fréedericksz transition.

As MLC 2081 was negative throughout its nematic range, the elastic constants was obtained by fitting $\varepsilon(V)$ in the HT device at a variety of temperatures. Due to the change in sign $\Delta\varepsilon$ for dimer mixture $M_{60:40:0}$ at a crossover temperature of 63 °C, a HT device was used to determine elastic constants below and a PH (planar homogeneous) device was used above this temperature, respectively (S1 includes examples of the fitted data). The values of the elastic constants obtained are shown in Fig. 4c, where errors are taken from the combined error in values of $|\Delta\varepsilon|$ and V_C. Here, as $\Delta\varepsilon$ became very small closer to the crossover temperature of 63 °C, only a limited region of the entire Fréedericksz transition was studied. This resulted in a considerably higher experimental uncertainties around this region (shown as hollow symbols). In Fig. 4c, both k_{11} and k_{33} of MLC 2081 and k_{11} of $M_{60:40:0}$ are fitted to the square of the nematic order parameter estimated from the Maier–Saupe theory, calculated using:[107]

$$k_{ii} = k_{ii}^0\left(1 - \frac{T}{T^*}\right)^{2\Upsilon}, \quad i = 1, 3 \qquad (13)$$

where k_{ii}^0 are the values of the elastic constant as temperature T tends to zero kelvin and T^* is the temperature from which second order phase transition behaviour is calculated. The values $\Upsilon = 0.225$ and $T^* = 1.023$. T_{NI} were found by fitting to numerical predictions of the Maier–Saupe theory.[108,109] (Table S1, ESI† gives fitting values). It is evident in Fig. 4c that the addition of CB7CB has decreased the magnitude of both k_{11} and k_{33}, and that k_{11}/k_{33} is greatly increased. The k_{33} for $M_{60:40:0}$ does not follow the Maier–Saupe relation (eqn (13)) and is found to have the opposite temperature dependence of decreasing magnitude with increasing order parameter. Similar behaviour has been observed in other bent dimeric compounds and their mixtures with calamitic materials previously.[60,70,90] The origin of this is sometimes considered to be caused by stiffening of the alkyl spacer unit, which leads to the banana shaped conformer of the dimer molecules becoming favoured and hence dielectrically negative. Correspondingly, the banana-shaped conformer favours bend deformations thereby reducing k_{33}.[66]
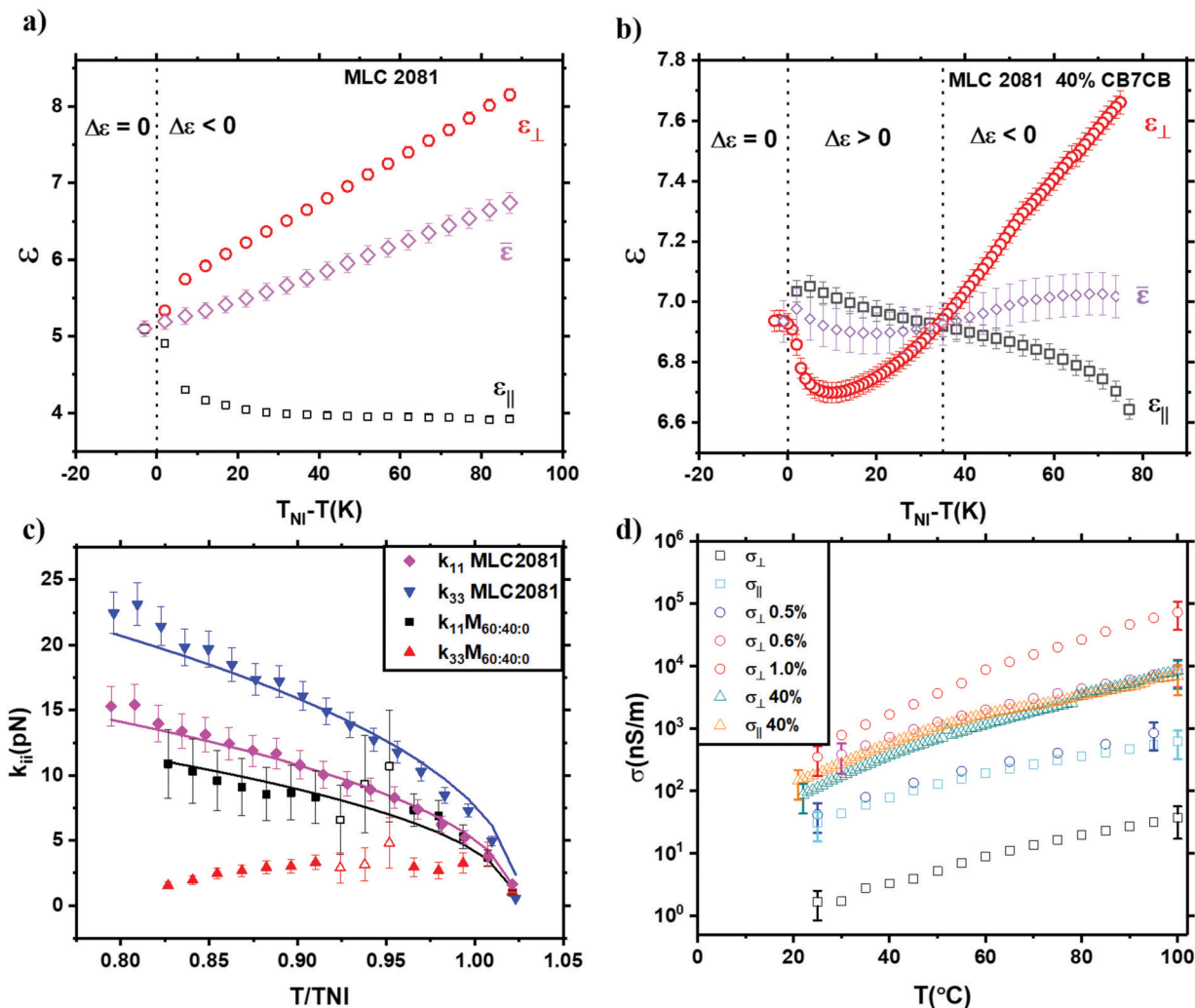
Fig. 4 Plot of ε for (a) MLC 2081 and (b) its mixture with the odd-dimer CB7CB ($M_{60:40:0}$). (c) A plot of the splay (k_{11}) and bend (k_{33}) elastic constants as functions of reduced temperature in MLC2081 and $M_{60:40:0}$. Both k_{11} and k_{33} values in MLC 2081 and k_{11} in $M_{60:40:0}$ are fitted with a Maier–Saupe type expression. Points close to the temperature where $\Delta\varepsilon$ is close to zero in $M_{60:40:0}$ ($T = 63\ ^\circ$C) are indicated by hollow symbols and have higher uncertainties associated with the elastic constant measurements. (d) Shows the temperature dependence of the conductivity for the samples for pure MLC 2081 (squares), MLC 2081 doped with TBATPB (circles) and MLC 2081 doped with CB7CB (triangles), and the dopant concentration is given in the key. Error bars are only indicated in highest and lowest temperatures for clarity.

As discussed in earlier sections, for an NLC to adopt the NR mode of EHDI, sufficient ion flow is required to produce a torque that destabilises the uniformly aligned director.[34,36,39,40] Fig. 4d shows plots of σ as a function of temperature for pure MLC 2081 TBATPB and CB7CB doped samples ($M_{100:0:X}$ materials and $M_{60:40:0}$). It is clear from the data that the addition of the salt TBATPB dramatically increases the σ values compared to pure MLC 2081 as intended, thereby enabling mixtures with similar conducitivies to be compared. As reported previously, the TBATPB appears to degrade HT alignment layer meaning values $\sigma_{\parallel}$ were not possible to find accurately.[31] It can be seen that in $M_{60:40:0}$ the addition of CB7CB increased the conductivity of the mixture compared to pure MLC 2081, this conductivity was sufficient in $M_{60:40:0}$ to undergo EHDI without the addition of TBATPB. It was also noted that above around 75 °C, the mixture $M_{60:40:0}$ changed sign $\Delta\sigma$ from positive to negative. This behaviour

is interesting and may be due to the same change in ratio of hairpin and banana conformer that leads to the change in sign $\Delta\varepsilon$ at 63 °C and the anomalous temperature dependence for k_{33} of the mixture.

EHDI characterisation

The NR mode EHDI behaviour of devices 3–7 was investigated in detail. The critical voltage and wave-vectors V_C and q_C were measured as functions of frequency for temperatures across the nematic range where $\Delta\varepsilon$ is negative. Although EHDI was observable in the dimer mixture $M_{60:40:0}$ while $\Delta\varepsilon$ was positive, the patterns were highly transient over time as found previously,[106] due to the competition between Fréedericksz reorientation and the formation of EHDI rolls. In this case, the situation is further complicated by the crossover in $\Delta\sigma$.

In the NR mode, the values of V_C and q_C in all samples behaved in the manner described by eqn (10) and (11). Here at a given frequency, f_{diel}, the onset pattern (at V_C) would change from the NR mode into the chevron pattern (see Fig. 1c). As has been previously observed this transition appears to consistently occur in standard calamitics at a frequency where $\lambda = d/2$,[31,50–53] leading to the limits of continuous variation given in eqn (4). A possible reason for such behaviour could be a similar effect to that described by Penz and Ford,[45] where due to a reduction in roll pitch a favourable hydrodynamic solution can be attained by partially overlaying two rolls above one another. Further work to confirm such a possibility within the structure of the standard model, is required.

Fig. 2d shows the hypothesis leading to this paper, where by creating a bent dimeric mixture with unusually low elastic constant k_{33} the rolls will become more ovular, allowing greater values q_C than those given in eqn (4). To examine this, the devices were tested at several temperatures across their nematic range to observe the NR mode at a wide range of k_{11}, k_{33} and their ratio. Fig. 5 shows an example comparison of V_C and q_C values for the NR mode in devices 4 and 7, which are filled with the ion-doped $M_{100:0:0.5}$ and bent dimer doped $M_{60:40:0}$ respectively. V_C and q_C are shown at several temperatures as functions of frequency while maintaining the NR state. These two devices were chosen for comparison because of the similar spacing (~ 20 μm) and conductivity (~ 100 nS m^{-1} at 30 °C) yet they display significantly different values of q_C and V_C. The lines in the figure represent best fits of the data points to eqn (10) and (11), respectively. As the temperature is increased, the divergences shift to higher f_{crit} values. This shift was observed previously and attributed to a higher number and mobility of the available charge carriers in the material at higher temperatures.[31,56]

Comparing Fig. 5a, b and c, d, it is suggested that the manipulation of elastic constants caused by the addition of the CB7CB has led to significantly different values of V_C and q_C.
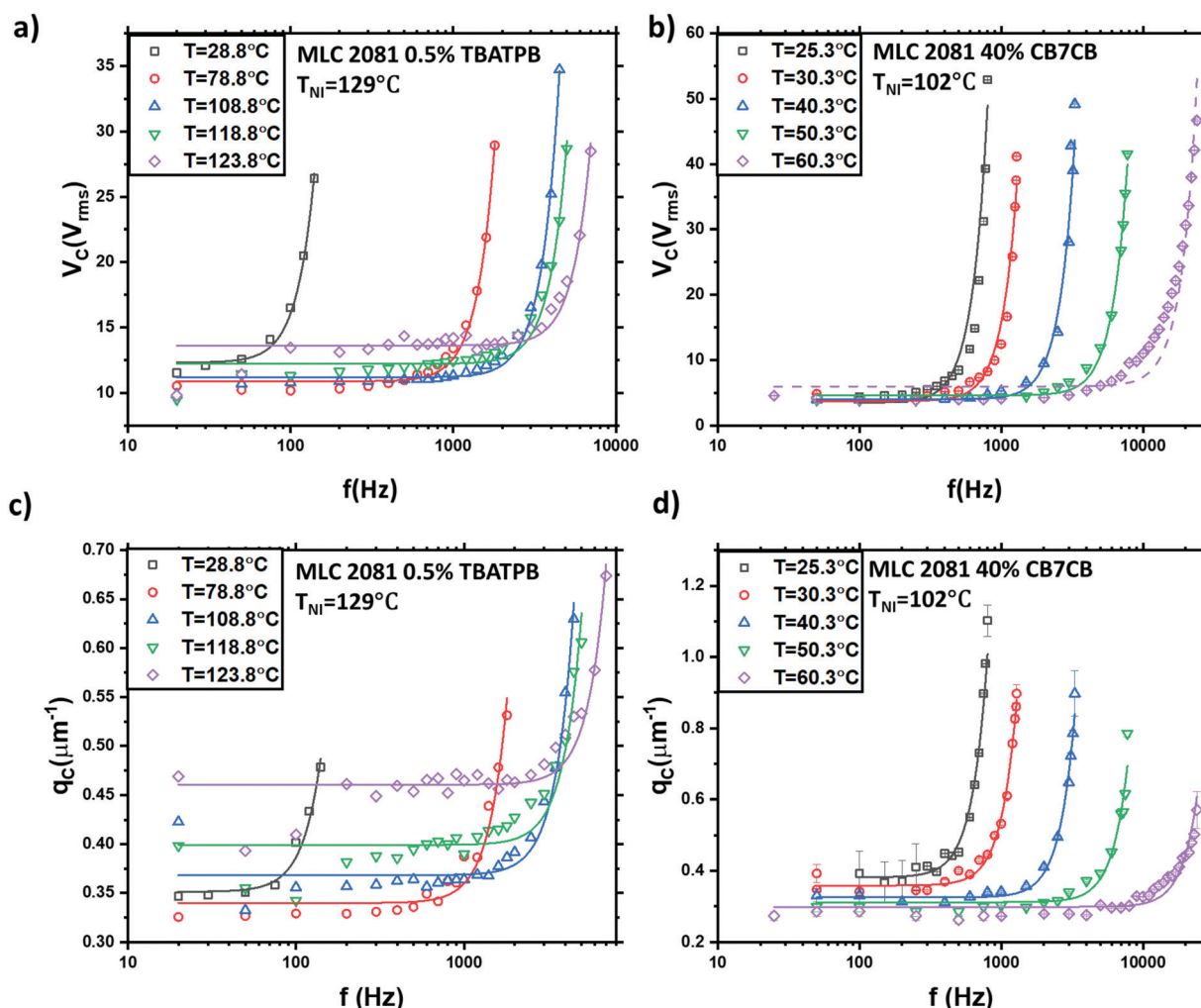

Fig. 5 V_C and q_C curves for pure MLC 2081 (w/0.5% TBATPB) and the MLC 2081 with 40% CB7CB in ~ 20 μm spaced devices (device 4 and 7 in Table 1). These only show values while the device maintained NR 1D diffractive structure. (a) and (b) show measured values of V_C fitted with eqn (10), the dashed line in (b) indicates a poor fit, which only occurs in CB7CB doped sample when $\Delta\varepsilon$ is exceptionally small. (c) and (d) show the same but for q_C values fitted with eqn (11).
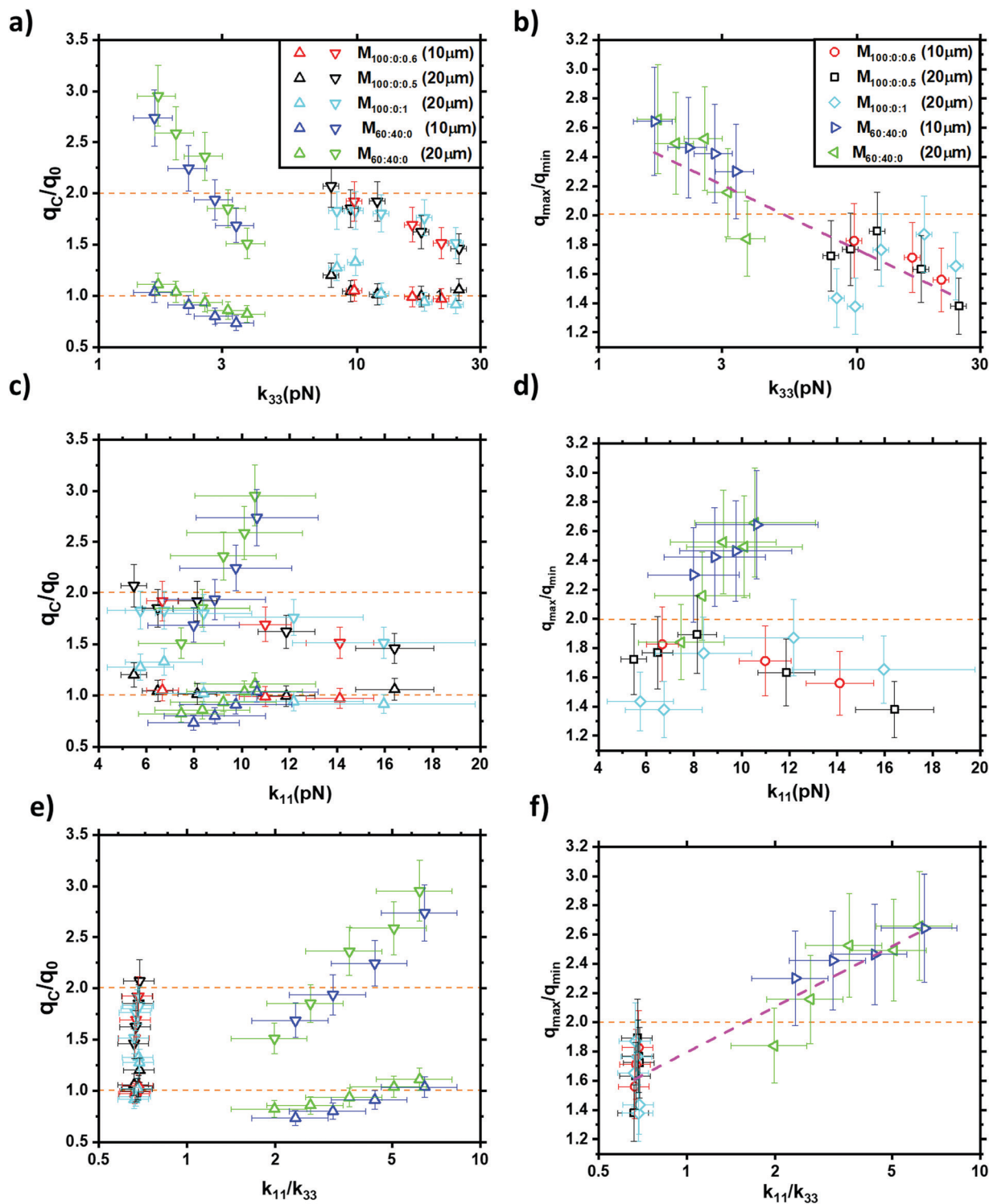
Fig. 6 Shows quantities related to q_C as a function of elastic constants and their ratios. (a) Gives the key for all samples. The left side (a, c and e) plots show the maximum (downward triangles) and minimum (upward triangles) values of q_C observed to form a uniform NR grating as the frequency was varied. The q_C values are normalised by q_0. The orange dotted lines represent the expected range of q_C values according to eqn (4), where only the samples with CB7CB in are outside of them. The right side (b, d and f) shows the ratio of the q_{max} and the q_{min}. The horizontal orange dotted line shows only samples with CB7CB have a value of q_{max}/q_{min} greater than 2. In (b) and (f), the most continuous behaviour between the MLC 2081 and $M_{60:40:0}$ was observed; here, concatenated fits are used to guide the eye.

From the examples given in Fig. 5 it can be seen that the dimer doped system has significantly lower V_C values in the range 4 ± 2 V while the ion doped system is around 3 times this at 12 ± 2 V. Similarly the dimer doped mixture displays significantly
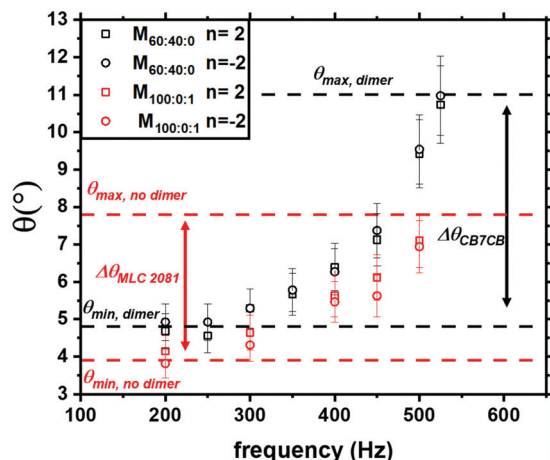
Fig. 7 Plot comparing the steering angles of the dominant $n = 2$ diffraction order of devices undergoing EHDI in MLC 2081 with 1% TBATPB and MLC 2081 with 40% CB7CB (devices 5 and 7 in Table 1 respectively). Despite similar spacings, the device with CB7CB demonstrates considerably wider angle steering.

larger maximum q_C values as was predicted. This is considered in more detail in the Discussion section.

Effect of elastic constants on EHDI pitch

Fig. 6 shows the plots of the largest (q_{max}) and smallest (q_{min}) values observed for an NR grating in each of the devices in Table 1. The data demonstrate the causal link between the changes in elastic constants and the observed q_C values. Here each quantity is normalised to q_0 ($= 2\pi/d$) and the ratios plotted against the elastic constants and k_{11}/k_{33}. From these plots, it is clear that only the mixture including the bent dimer ($M_{60:40:0}$) is outside the limits given in eqn (4), with new limits of approximately,

$$q_0 \times 75\% \leq q_C \leq 2q_0 \times 150\%. \tag{14}$$

The new limits indicate the possibility of wider angle steering in the mixtures containing the dimer material. To confirm this diffraction analysis of the devices 5 (no dimer sample) and 7 (with dimer) was carried out. Fig. 7 is the plot of the steering angle for the dominant $n = 2$ diffraction order. It is clear from the plot that in the dimer doped device both the angles (θ_{min}, θ_{max}) and their range ($\Delta\theta$) have increased due to larger values of q_C.

Further, Fig. 6a and b show that lower k_{33} values tend to exhibit the most considerable disagreement with eqn (4), while higher values are always inside the limits. Fig. 6c and d, show how the q_C ranges change with, k_{11}, where the effect is less clear, possibly due to the changes in q_C being dominated by k_{33}. Fig. 6e and f, show this data as functions of k_{11}/k_{33}, which seems to indicate a trend of higher q_C values and range as k_{11}/k_{33} is increased as previously predicted.[31]

From each of these graphs, it is apparent that the concentration of TBATPB does not change values of q_C displayed, provided there are sufficient ions for the system to undergo NR mode EHDI. Similarly, the device spacing does not change the

limits of q_C in either the CB7CB or the TBATPB doped MLC 2081, once the results are normalised by q_0.

Discussion

So far, we focussed on the effect of varying material elastic constants to increase the values of q_C and reduce V_C. However, the results also show that the addition of CB7CB also change the material's dielectric and resistive properties (ε and σ in Fig. 4), in addition to probable changes in unmeasured viscosity. To establish that the effects mentioned are due to change in elastic constants, let us consider the likely effect of these other factors on the behaviour of V_C and q_C, separately.

Behaviour of V_C

Firstly to assess the observed changes in V_C consider the model of Kramer and Pesch,[44,47]

$$\varepsilon_0 V_C^2 = \frac{\pi^2 K_{eff}}{\Delta\varepsilon_{eff} + \varepsilon_\perp \cdot \frac{\alpha_2}{\eta_{eff}} \cdot \frac{\Delta\sigma_{eff}}{\sigma_\perp}} \tag{15}$$

where α_2 is the Leslie–Erickson flow viscosity coefficient that is approximately the negative of the rotational viscosity γ_1,[107] and $\Delta\varepsilon_{eff}$ and $\Delta\sigma_{eff}$, K_{eff}, are the effective dielectric and conductivity anisotropies and elastic constant respectively.

Although conductivity is included in eqn (15) it is unlikely that it is playing a dominant role in behaviour of V_C for the dimer doped mixture. In the ion doping experiments (e.g. $M_{100:0:0.5}$ and $M_{100:0:1}$[31]) the conductivity values increase through nearly three orders of magnitude without a substantial change of low-frequency V_C, while only a factor of three change is incurred in $M_{60:40:0}$ (which has a intermediate conductivity of $M_{100:0:0.5}$ and $M_{100:0:1}$). In contrast to conductivity, dielectric anisotropy is likely to play an important role in the reduction of V_C. This is due to the lower value of $|\Delta\varepsilon|$ in $M_{60:40:0}$ reducing the stabilising torque imposed by the applied electric field on the director compared to that of MLC 2081 (reducing the negativity of the first term in the denominator of eqn (15)). Finally, although difficult to conclude about the effect of viscosity without a direct measurement, the addition of the dimer should increase the mixture viscosity and hence increase V_C. This, in addition to the fact that samples were examined at a large range of temperatures with fairly small changes in V_C indicates the role of the strongly temperature dependent viscosity, is small. These observations lead us to conclude that the reduction in V_C is likely dominated by the dual effects of lowering the elastic term k_{eff} (mainly due to the reduction of k_{33}) and reduction of the negative $|\Delta\varepsilon|$.

Behaviour of q_C

Similarly to the arguments for V_C given above, it is unlikely that observed changes to q_C range were caused by changing conductivity as this was not observed when examining different ion concentrations, with orders of magnitude variation in conductivity.[31] Unlike the effect on V_C, the reduction of minimum feature size defined by q_C is not caused by changes to $\Delta\varepsilon$.

This has been shown in previous works,[29,35] where it had been noted that a smaller $|\Delta\varepsilon|$ is likely to decrease q_C values. This may allow q_C for $M_{60:40:0}$ shown in Fig. 6 to go below the lower limits of eqn (4), but can not lead to rolls that surpass the upper limit. This supports the argument that the observed large q_C values seen in the dimer doped mixtures are dominated by the changes to the elastic properties. Samples without dimer were tested at many temperatures and ionic dopant levels, covering a wide range of values of σ, ε and viscosity but none of them showed $q_C > 2q_0$.

Role of flexoelectricity

Another potential material parameter that can influence the formation of EHDIs is the flexoelectric coefficients. CB7CB has been reported to have forty times higher flexoelastic coefficient values compared to standard calamitics[108] so the mixture $M_{60:40:0}$ is likely also to have significantly increased flexoelectric coefficients (particularly e_3). The EHDI analysis by Tavener et al.[29] using the standard model does not include flexoelectric terms, and without such modelling methods, prediction of their effects on observed V_C and q_C values is difficult. However, it is unlikely that they are responsible for the observed change in the conduction regime, where such effects should be magnitudes smaller than the ionic effects.[83–85,109,110] Flexoelectric rolls are observed in both bent-core and odd-dimer liquid crystals.[111–113] However, it is unlikely the rolls investigated here are flexoelectric in origin since they depend strongly on sample conductivity,[81] have the normal parallel to the director,[82] and have a different frequency and voltage dependence of the onset behaviour.[114–117] All mixtures studied here follow the predictions for the NR mode, indicating these flexoelectric terms are unlikely playing a significant role in the observed behaviour.[58,61,81–83]

Conclusion

This paper demonstrates the influence of LC elastic constants on the pitch of the grating structures in nematic EHDIs. New nematic mixtures are designed by adding an odd-spaced bent dimeric nematic liquid crystal to a typical host calamitic NLC to deliberately change the elastic properties while maintaining negative $\Delta\varepsilon$. EHDI are induced in a variety of mixtures and a systematic study of the influence of material properties on the grating formation is provided. In our previous work,[31] it was predicted that a possible methodology of reducing λ_C values would be to create materials with significantly lower k_{33}. The current work supports this hypothesis and demonstrates the ability of such low k_{33} values to increase q_C values to higher than $2q_0$, which a standard calamitic NLC cannot usually achieve.

This work acknowledges that, although the change in k_{33} is the principal candidate for the observed effects, there is also the possibility that changes in the material's viscosities, permittivities, conductivities or flexoelectric coefficients could also contribute to these changes. However, arguments are presented

that suggest the change is dominated by the large reduction of k_{33} associated with the odd-spaced dimer.

Although LC systems undergoing EHDI have been considered unsuited in their ability to be applied to real-world devices compared to systems such as LCoS, this work demonstrates their ability to create well-ordered grating structures with sub 4 μm features, which are comparable to the limits of LCoS reflective devices, with the additional advantages of operating in transmissive mode and being continually variable. We demonstrate that as the frequency is increased, in a 10 μm spaced device, λ varies from 7 to 3.5 μm. This created a continuous angular variation from ~9 to 21°, although reduction in efficiency at higher steering angles was observed.[31] It should also be noted that the demonstrated technique of lowering k_{33} could also have application in other types of grating formation based on a hydrodynamic phenomenon, or in increasing the stability of structures that have a similar desired director conformation.

Conflicts of interest

There are no conflicts to declare.

Acknowledgements

References

1 M. Schadt and W. Helfrich, Voltage-dependent optical activity of a twisted nematic liquid crystal, Appl. Phys. Lett., 1971, 18, 127–128, DOI: 10.1063/1.1653593.

2 G. H. Heilmeier, L. A. Zanoni and L. A. Barton, Dynamic scattering in nematic liquid crystals, Appl. Phys. Lett., 1968, 13, 46–47, DOI: 10.1063/1.1652453.

3 U. Efron, J. Grinberg, P. O. Braatz, M. J. Little, P. G. Reif and R. N. Schwartz, The silicon liquid-crystal light valve, J. Appl. Phys., 1985, 57, 1356–1368, DOI: 10.1063/1.334487.

4 P. F. McManamon, T. A. Dorschner, D. L. Corkum, L. J. Friedman, D. S. Hobbs, M. Holz, S. Liberman, H. Q. Nguyen, D. P. Resler, R. C. Sharp and E. A. Watson, Optical phased array technology, Proc. IEEE, 1996, 84, 268–298, DOI: 10.1109/5.482231.

5 P. F. McManamon, P. J. Bos, M. J. Escuti, J. Heikenfeld, S. Serati, H. Xie and E. A. Watson, A Review of Phased Array Steering for Narrow-Band Electrooptical Systems, Proc. IEEE, 2009, 97, 1078–1096, DOI: 10.1109/JPROC.2009.2017218.

6 G. D. Love, Wave-front correction and production of Zernike modes with a liquid-crystal spatial light modulator, Appl. Opt., 1997, 36, 1517–1520, DOI: 10.1364/ao.36.001517.

7 L. Hu, L. Xuan, Y. Liu, Z. Cao, D. Li and Q. Mu, Phase-only liquid crystal spatial light modulator for wavefront

correction with high precision, *Opt. Express*, 2004, **12**, 6403, DOI: 10.1364/OPEX.12.006403.

8 Z. Zhang, Z. You and D. Chu, Fundamentals of phase-only liquid crystal on silicon (LCOS) devices, *Light: Sci. Appl.*, 2014, **3**, e213, DOI: 10.1038/lsa.2014.94.

9 L. Susumu Sato, A. Sugiyama, R. Sato, S. Sato, L. Susumu Sato, A. Sugiyama, R. Sato and S. Sato, Liquid-crystal lens-cells with variable focal length, *Jpn. J. Appl. Phys.*, 1979, **18**, 1679–1684, DOI: 10.1143/JJAP.18.1679.

10 S. Sato, Applications of Liquid Crystals to Variable-Focusing Lenses, *Opt. Rev.*, 1999, **6**, 471–485, DOI: 10.1007/s10043-999-0471-z.

11 H.-C. Lin, M.-S. Chen and Y.-H. Lin, A Review of Electrically Tunable Focusing Liquid Crystal Lenses, *Trans. Electr. Electron. Mater.*, 2011, **12**, 234–240, DOI: 10.4313/TEEM.2011.12.6.234.

12 R. G. Lindquist, T. M. Leslie, J. H. Kulick, G. P. Nordin, J. M. Jarem, S. T. Kowel and M. Friends, High-resolution liquid-crystal phase grating formed by fringing fields from interdigitated electrodes, *Opt. Lett.*, 1994, **19**, 670, DOI: 10.1364/OL.19.000670.

13 J. Kim, C. Oh, S. Serati and M. J. Escuti, Wide-angle, nonmechanical beam steering with high throughput utilizing polarization gratings, *Appl. Opt.*, 2011, **50**, 2636, DOI: 10.1364/AO.50.002636.

14 N. Mukohzaka, N. Yoshida, H. Toyoda, Y. Kobayashi and T. Hara, Diffraction efficiency analysis of a parallel-aligned nematic-liquid-crystal spatial light modulator, *Appl. Opt.*, 1994, **33**, 2804, DOI: 10.1364/AO.33.002804.

15 R. A. Kashnow and J. E. Bigelow, Diffraction from a Liquid Crystal Phase Grating, *Appl. Opt.*, 1973, **12**, 2302, DOI: 10.1364/AO.12.002302.

16 Z. He, F. Gou, R. Chen, K. Yin, T. Zhan and S.-T. Wu, Liquid Crystal Beam Steering Devices: Principles, Recent Advances, and Future Developments, *Crystals*, 2019, **9**, 292, DOI: 10.3390/cryst9060292.

17 R. M. Matic, Blazed phase liquid crystal beam steering, in *Laser Beam Propagation and Control*, ed. H. Weichel and L. F. DeSandre, International Society for Optics and Photonics, Los Angeles, 1994, pp. 194–205.

18 X. Wang, D. Wilson, R. Muller, P. Maker and D. Psaltis, Liquid-crystal blazed-grating beam deflector, *Appl. Opt.*, 2000, **39**, 6545, DOI: 10.1364/AO.39.006545.

19 J. Stockley and S. Serati, Advances in liquid crystal beam steering, in *Free-Space Laser Communications IV*, ed. J. C. Ricklin and D. G. Voelz, 2004, p. 32.

20 X. Wang, B. Wang, J. Pouch, F. Miranda, M. Fisch, J. E. Anderson, V. Sergan and P. J. Bos, Liquid crystal on silicon(LCOS) wavefront corrector and beam steerer, *Proc. SPIE*, 2003, **5162**, 139–146, DOI: 10.1117/12.511504.

21 K. M. Johnson, D. J. McKnight and I. Underwood, Smart Spatial Light Modulators Using Liquid Crystals on Silicon, *IEEE J. Quantum Electron.*, 1993, **29**, 699–714, DOI: 10.1109/3.199323.

22 D. J. McKnight, K. M. Johnson and R. A. Serati, 256 × 256 liquid-crystal-on-silicon spatial light modulator, *Appl. Opt.*, 1994, **33**, 2775, DOI: 10.1364/AO.33.002775.

23 V. Fréedericksz and V. Zolina, Forces causing the orientation of an anisotropic liquid, *Trans. Faraday Soc.*, 1933, **29**, 919–930, DOI: 10.1039/TF9332900919.

24 P. G. de Gennes and J. Prost, Static Distortions in Nematic Liquid Crystal, *The Physics of Liquid Crystals*, Oxford University Press, 1993, pp. 98–162.

25 F. C. Frank, On the theory of liquid crystals, *Discuss. Faraday Soc.*, 1958, **25**, 19, DOI: 10.1039/df9582500019.

26 C. W. Oseen, The theory of liquid crystals, *Trans. Faraday Soc.*, 1933, **29**, 883, DOI: 10.1039/tf9332900883.

27 P. G. de Gennes and J. Prost, Dynamical Properties of Nematics, in *The Physics of Liquid Crystals*, Oxford University Press, 1993, pp. 198–262.

28 N. V. Madhusudana, Electroconvective instabilities in nematic liquid crystals, *Phase Transitions*, 1994, **50**, 177–191, DOI: 10.1080/01411599408200373.

29 S. J. Tavener, T. Mullin, G. I. Blake and K. A. Cliffe, Numerical bifurcation study of electrohydrodynamic convection in nematic liquid crystals, *Phys. Rev. E: Stat., Nonlinear, Soft Matter Phys.*, 2001, **63**, 1–12, DOI: 10.1103/PhysRevE.63.011708.

30 A. Buka, Pattern Formation in Liquid Crystals, *Phys. Scr.*, 1989, 114–117, DOI: 10.1088/0031-8949/1989/T25/019.

31 R. Morris, J. C. Jones and M. Nagaraj, Continuously variable diffraction gratings using electroconvection in liquid crystals for beam steering applications, *J. Appl. Phys.*, 2019, **126**, 224505, DOI: 10.1063/1.5128205.

32 R. Williams, Domains in Liquid Crystals, *J. Chem. Phys.*, 1963, **39**, 384–388, DOI: 10.1063/1.1734257.

33 R. Williams, Liquid crystals in an electric field, *Nature*, 1963, **199**, 273–274, DOI: 10.1038/199273a0.

34 E. Dubois-Violette, P. G. de Gennes and O. Parodi, Hydrodynamic instabilities of nematic liquid crystals under A. C. electric fields, *J. Phys.*, 1971, **32**, 305–317, DOI: 10.1051/jphys:01971003204030500.

35 A. Buka, N. Éber, W. Pesch and L. Kramer, Convective Patterns in Liquid Crystals Driven by an Electric Field, *Advances in Sensing with Security Applications*, Kluwer Academic Publishers, Dordrecht, 2005, pp. 55–82.

36 Orsay Liquid Crystal Group, Hydrodynamic instabilities in nematic liquids under ac electric fields, *Phys. Rev. Lett.*, 1970, **25**, 1642–1643, DOI: 10.1103/PhysRevLett.25.1642.

37 T. John, U. Behn and R. Stannarius, Laser diffraction by periodic dynamic patterns in anisotropic fluids, *Eur. Phys. J. B*, 2003, **35**, 267–278, DOI: 10.1140/epjb/e2003-00277-1.

38 C. Bohley, J. Heuer and R. Stannarius, Optical properties of electrohydrodynamic convection patterns: rigorous and approximate methods, *J. Opt. Soc. Am. A*, 2005, **22**, 2818, DOI: 10.1364/JOSAA.22.002818.

39 E. F. Carr, Influence of Electric Fields on the Molecular Alignment in the Liquid Crystal p -(Anisalamino)-phenyl Acetate, *Mol. Cryst.*, 1969, **7**, 253–268, DOI: 10.1080/15421406908084876.

40 W. Helfrich, Conduction-Induced Alignment of Nematic Liquid Crystals: Basic Model and Stability Considerations, *J. Chem. Phys.*, 1969, **51**, 4092–4105, DOI: 10.1063/1.1672632.

41 L. Kramer and W. Pesch, Convection Instabilities in Nematic Liquid Crystals, *Annual Review of Fluid Mechanics*, 2006, pp. 515–539.

42 E. Guyon and P. Pieranski, Convective instabilities in nematic liquid crystals, *Physica*, 1974, **73**, 184–194, DOI: 10.1016/0031-8914(74)90234-1.

43 E. Bodenschatz, W. Zimmermann and L. Kramer, On electrically driven pattern-forming instabilities in planar nematics On electrically driven pattern-forming instabilities in planar nematics, *J. Phys.*, 1988, **49**, 1875–1899, DOI: 10.1051/jphys:0198800490110187500＞.

44 A. Buka, N. Eber, W. Pesch and L. Kramer, Convective Patterns in Liquid Crystal Driven by Electric Field, *Advances in sensing with security applications. NATO Science Series II: Mathematics, Physics and Chemistry*, 2006, vol. 218, pp. 55–82, DOI: 10.1007/1-4020-4355-4_02.

45 P. A. Penz and G. W. Ford, Electromagnetic Hydrodynamics of Liquid Crystals, *Phys. Rev. A: At., Mol., Opt. Phys.*, 1972, **6**, 414–425, DOI: 10.1103/PhysRevA.6.414.

46 E. Kochowska, S. Németh, G. Pelzl and Á. Buka, Electroconvection with and without the Carr-Helfrich effect in a series of nematic liquid crystals, *Phys. Rev. E: Stat., Nonlinear, Soft Matter Phys.*, 2004, **70**, 011711, DOI: 10.1103/PhysRevE.70.011711.

47 L. Kramer and W. Pesch, Electrohydrodynamic Instabilities in Nematic Liquid Crystals, *Pattern Formation in Liquid Crystals*, 1996, pp. 221–255.

48 E. Dubois-Violette, Theory of instabilities of nematics under A. C electric fields: Special effects near the cut off frequency, *J. Phys.*, 1972, **33**, 95–100, DOI: 10.1051/jphys:0197200330109500.

49 L. M. Blinov and V. G. Chigrinov, *Electrooptic Effects in Liquid Crystal Materials*, Springer New York, New York, NY, 1994.

50 M. Scheuring, L. Kramer and J. Peinke, Formation of chevrons in the dielectric regime of electroconvection in nematic liquid crystals, *Phys. Rev. E*, 1998, **58**, 2018–2026, DOI: 10.1103/PhysRevE.58.2018.

51 N. Oikawa, Y. Hidaka and S. Kai, Formation of a defect lattice in electroconvection of nematics, *Phys. Rev. E: Stat., Nonlinear, Soft Matter Phys.*, 2004, **70**, 6, DOI: 10.1103/PhysRevE.70.066204.

52 H. Bohatsch and R. Stannarius, Frequency-induced structure transition of nematic electroconvection in twist cells, *Phys. Rev. E: Stat. Phys., Plasmas, Fluids, Relat. Interdiscip. Top.*, 1999, **60**, 5591–5599, DOI: 10.1103/PhysRevE.60.5591.

53 J. H. Huh, Y. Hidaka, A. G. Rossberg and S. Kai, Pattern formation of chevrons in the conduction regime in homeotropically aligned liquid crystals, *Phys. Rev. E: Stat. Phys., Plasmas, Fluids, Relat. Interdiscip. Top.*, 2000, **61**, 2769–2776, DOI: 10.1103/PhysRevE.61.2769.

54 S. Kaur, Elastic properties of bent-core nematic liquid crystals: the role of the bend angle, *Liq. Cryst.*, 2016, **43**, 2277–2284, DOI: 10.1080/02678292.2016.1232442.

55 S. Kaur, J. Addis, C. Greco, A. Ferrarini, V. Görtz, J. W. Goodby and H. F. Gleeson, Understanding the distinctive elastic constants in an oxadiazole bent-core nematic liquid crystal, *Phys. Rev. E: Stat., Nonlinear, Soft Matter Phys.*, 2012, **86**, 41703, DOI: 10.1103/PhysRevE.86.041703.

56 S. Tanaka, H. Takezoe, N. Éber, K. Fodor-Csorba, A. Vajda and Á. Buka, Electroconvection in nematic mixtures of bent-core and calamitic molecules, *Phys. Rev. E: Stat., Nonlinear, Soft Matter Phys.*, 2009, **80**, 021702, DOI: 10.1103/PhysRevE.80.021702.

57 P. Sathyanarayana, M. Mathew, Q. Li, V. S. S. S. Sastry, B. Kundu, K. V. Le, H. Takezoe and S. Dhara, Splay bend elasticity of a bent-core nematic liquid crystal, *Phys. Rev. E: Stat., Nonlinear, Soft Matter Phys.*, 2010, **81**, 010702, DOI: 10.1103/PhysRevE.81.010702.

58 Y. Xiang, J. W. Goodby, V. Görtz and H. F. Gleeson, Revealing the uniaxial to biaxial nematic liquid crystal phase transition via distinctive electroconvection, *Appl. Phys. Lett.*, 2009, **94**, 193507, DOI: 10.1063/1.3138867.

59 D. Shen, A. Pegenau, S. Diele, I. Wirth and C. Tschierske, Molecular Design of Nonchiral Bent-Core Liquid Crystals with Antiferroelectric Properties, *J. Am. Chem. Soc.*, 2000, **122**, 1593–1601, DOI: 10.1021/ja993572w.

60 M. Majumdar, P. Salamon, A. Jákli, J. T. Gleeson and S. Sprunt, Elastic constants and orientational viscosities of a bent-core nematic liquid crystal, *Phys. Rev. E*, 2011, **83**, 31701, DOI: 10.1103/PhysRevE.83.031701.

61 A. Jákli, Liquid crystals of the twenty-first century – nematic phase of bent-core molecules, *Liq. Cryst. Rev.*, 2013, **1**, 65–82, DOI: 10.1080/21680396.2013.803701.

62 G. Dantlgraber, A. Eremin, S. Diele, A. Hauser, H. Kresse, G. Pelzl and C. Tschierske, Chirality and Macroscopic Polar Order in a Ferroelectric Smectic Liquid-Crystalline Phase Formed by Achiral Polyphilic Bent-Core Molecules, *Angew. Chem., Int. Ed.*, 2002, **41**, 2408, DOI: 10.1002/1521-3773(20020703)41:13＜2408::AID-ANIE2408＞3.0.CO;2-M.

63 I. Dozov, On the spontaneous symmetry breaking in the mesophases of achiral banana-shaped molecules, *Europhys. Lett.*, 2001, **56**, 247–253, DOI: 10.1209/epl/i2001-00513-x.

64 C. Meyer, G. R. Luckhurst and I. Dozov, Flexoelectrically Driven Electroclinic Effect in the Twist-Bend Nematic Phase of Achiral Molecules with Bent Shapes, *Phys. Rev. Lett.*, 2013, **111**, 067801, DOI: 10.1103/PhysRevLett.111.067801.

65 J. Etxebarria and M. Blanca Ros, Bent-core liquid crystals in the route to functional materials, *J. Mater. Chem.*, 2008, **18**, 2919, DOI: 10.1039/b803507e.

66 K. Adlem, M. Copič, G. R. Luckhurst, A. Mertelj, O. Parri, R. M. Richardson, B. D. Snow, B. A. Timimi, R. P. Tuffin and D. Wilkes, Chemically induced twist-bend nematic liquid crystals, liquid crystal dimers, and negative elastic constants, *Phys. Rev. E: Stat., Nonlinear, Soft Matter Phys.*, 2013, **88**, 22503, DOI: 10.1103/PhysRevE.88.022503.

67 V. P. Panov, M. Nagaraj, J. K. Vij, Y. P. Panarin, A. Kohlmeier, M. G. Tamba, R. A. Lewis and G. H. Mehl, Spontaneous Periodic Deformations in Nonchiral Planar-Aligned Bimesogens with a Nematic-Nematic Transition and a Negative Elastic Constant, *Phys. Rev. Lett.*, 2010, **105**, 167801, DOI: 10.1103/PhysRevLett.105.167801.

68 G. Ungar, V. Percec and M. Zuber, Influence of molecular structure on the nematic-nematic transition in polyethers based on 1-(4-hydroxyphenyl)-2-(2-R-4-hydroxyphenyl)ethane where R = CH3 and Cl, and flexible spacers with an odd number of methylene units, *Polym. Bull.*, 1994, **32**, 325–330, DOI: 10.1007/BF00308544.

69 M. Cestari, S. Diez-Berart, D. A. Dunmur, A. Ferrarini, M. R. De La Fuente, D. J. B. Jackson, D. O. Lopez, G. R. Luckhurst, M. A. Perez-Jubindo, R. M. Richardson, J. Salud, B. A. Timimi and H. Zimmermann, Phase behavior and properties of the liquid-crystal dimer 1,7-bis(4-cyanobiphenyl-4-yl) heptane: A twist-bend nematic liquid crystal, *Phys. Rev. E: Stat., Nonlinear, Soft Matter Phys.*, 2011, **84**, 31704, DOI: 10.1103/PhysRevE.84.031704.

70 N. Sebastián, B. Robles-Hernández, S. Diez-Berart, J. Salud, G. R. Luckhurst, D. A. Dunmur, D. O. López and M. R. de la Fuente, Distinctive dielectric properties of nematic liquid crystal dimers, *Liq. Cryst.*, 2017, **44**(1), 177–190, DOI: 10.1080/02678292.2016.1218963.

71 K. L. Atkinson, S. M. Morris, F. Castles, M. M. Qasim, D. J. Gardiner and H. J. Coles, Flexoelectric and elastic coefficients of odd and even homologous bimesogens, *Phys. Rev. E: Stat., Nonlinear, Soft Matter Phys.*, 2012, **85**, 012701, DOI: 10.1103/PhysRevE.85.012701.

72 R. Balachandran, V. P. Panov, J. K. Vij, A. Kocot, M. G. Tamba, A. Kohlmeier and G. H. Mehl, Elastic properties of bimesogenic liquid crystals, *Liq. Cryst.*, 2013, **40**, 681–688, DOI: 10.1080/02678292.2013.765973.

73 R. J. Mandle, M. P. Stevens and J. W. Goodby, Developments in liquid-crystalline dimers and oligomers, *Liq. Cryst.*, 2017, **44**, 2046–2059, DOI: 10.1080/02678292.2017.1343500.

74 C. T. Imrie and P. A. Henderson, Liquid crystal dimers and higher oligomers: Between monomers and polymers, *Chem. Soc. Rev.*, 2007, **36**, 2096–2124, DOI: 10.1039/b714102e.

75 P. A. Henderson and C. T. Imrie, Methylene-linked liquid crystal dimers and the twist-bend nematic phase, *Liq. Cryst.*, 2011, **38**, 1407–1414, DOI: 10.1080/02678292.2011.624368.

76 V. Borshch, Y.-K. Kim, J. Xiang, M. Gao, A. Jákli, V. P. Panov, J. K. Vij, C. T. Imrie, M. G. Tamba, G. H. Mehl and O. D. Lavrentovich, Nematic twist-bend phase with nanoscale modulation of molecular orientation, *Nat. Commun.*, 2013, **4**, 2635, DOI: 10.1038/ncomms3635.

77 M. Cestari, E. Frezza, A. Ferrarini and G. R. Luckhurst, Crucial role of molecular curvature for the bend elastic and flexoelectric properties of liquid crystals: Mesogenic dimers as a case study, *J. Mater. Chem.*, 2011, **21**, 12303–12308, DOI: 10.1039/c1jm12233a.

78 D. A. Paterson, J. P. Abberley, W. T. Harrison, J. M. Storey and C. T. Imrie, Cyanobiphenyl-based liquid crystal dimers and the twist-bend nematic phase, *Liq. Cryst.*, 2017, **44**, 1–20, DOI: 10.1080/02678292.2016.1274293.

79 G. Babakhanova, Z. Parsouzi, S. Paladugu, H. Wang, Y. A. Nastishin, S. V. Shiyanovskii, S. Sprunt and O. D. Lavrentovich, Elastic and viscous properties of the nematic dimer CB7CB, *Phys. Rev. E*, 2017, **96**, 062704, DOI: 10.1103/PhysRevE.96.062704.

80 Z. Zhang, V. P. Panov, M. Nagaraj, R. J. Mandle, J. W. Goodby, G. R. Luckhurst, J. C. Jones, H. F. Gleeson and R. Spectroscopy, Raman scattering studies of order parameters in liquid crystal-line dimers exhibiting the nematic and twist-bend nematic phases, *J. Mater. Chem. C*, 2015, **3**, 10007–10016, DOI: 10.1039/c5tc02174j.

81 D. Wiant, J. T. Gleeson, N. Éber, K. Fodor-Csorba, A. Jákli and T. Tóth-Katona, Nonstandard electroconvection in a bent-core nematic liquid crystal, *Phys. Rev. E*, 2005, **72**, 041712, DOI: 10.1103/PhysRevE.72.041712.

82 S. Kaur, A. Belaissaoui, J. W. Goodby, V. Görtz and H. F. Gleeson, Nonstandard electroconvection in a bent-core oxadiazole material, *Phys. Rev. E: Stat., Nonlinear, Soft Matter Phys.*, 2011, **83**, 41704, DOI: 10.1103/PhysRevE.83.041704.

83 P. Tadapatri, U. S. Hiremath, C. V. Yelamaggad and K. S. Krishnamurthy, Patterned electroconvective states in a bent-core nematic liquid crystal, *J. Phys. Chem. B*, 2010, **114**, 10–21, DOI: 10.1021/jp9058802.

84 M. Petrov, E. Keskinova, B. Katranchev and H. Naradikian, Electroconvection in dimeric nematic liquid crystals with short-range smectic C order: dynamical characteristics, *Liq. Cryst.*, 2011, **38**, 41–52, DOI: 10.1080/02678292.2010.524944.

85 M. Petrov, B. Katranchev, E. Keskinova and H. Naradikian, The electroconvection in dimeric nematic liquid crystals, *J. Optoelectron. Adv. Mater.*, 2007, 438–441.

86 K. S. Krishnamurthy, N. B. Palakurthy and C. V. Yelamaggad, Confined Electroconvective and Flexoelectric Instabilities Deep in the Freedericksz State of Nematic CB7CB, *J. Phys. Chem. B*, 2017, **121**, 5447–5454, DOI: 10.1021/acs.jpcb.7b03072.

87 A. Krekhov, W. Pesch, N. Éber, T. Tóth-Katona and Á. Buka, Nonstandard electroconvection and flexoelectricity in nematic liquid crystals, *Phys. Rev. E: Stat., Nonlinear, Soft Matter Phys.*, 2008, **77**, 021705, DOI: 10.1103/PhysRevE.77.021705.

88 T. Tóth-Katona, N. Éber and Á. Buka, Flexoelectricity in Electroconvection, *Mol. Cryst. Liq. Cryst.*, 2009, **511**, 11/[1481]–24/[1494], DOI: 10.1080/15421400903048461.

89 W. Thom, W. Zimmermann and L. Kramer, The influence of the flexoelectric effect on the electrohydrodynamic instability in nematics, *Liq. Cryst.*, 1989, **4**, 309–316, DOI: 10.1080/02678298908029184.

90 L. M. Blinov, Domain Instabilities in liquid crystals, *J. Phys., Colloq.*, 1979, **40**, C3-247–C3-258, DOI: 10.1051/jphyscol:1979348.

91 Á. Buka, T. Toth-Katona, N. Éber, K. Alexei and W. Pasch, The Role of Flexoelectricity in Pattern Formation, in *Flexoelectricity in liquid crystals: Theory, experiments and applications*, ed. Á. Buka and N. Éber, Imperial College Press, 2010, pp. 101–129.

92 S. Srigengan, M. Nagaraj, A. Ferrarini, R. Mandle, S. J. Cowling, M. A. Osipov, G. Pająk, J. W. Goodby and H. F. Gleeson, Anomalously low twist and bend elastic constants in an oxadiazole-based bent-core nematic liquid crystal and its mixtures; contributions of spontaneous chirality and polarity, *J. Mater. Chem. C*, 2018, **6**, 980–988, DOI: 10.1039/C7TC04664B.

93 E. P. Raynes, C. V. Brown and J. F. Strömer, Method for the measurement of the K22 nematic elastic constant, *Appl. Phys. Lett.*, 2003, **82**, 13–15, DOI: 10.1063/1.1534942.

94 M. Cui and J. R. Kelly, Temperature Dependence of Visco-Elastic Properties of 5CB, *Mol. Cryst. Liq. Cryst. Sci. Technol., Sect. A*, 1999, **331**, 49–57, DOI: 10.1080/10587259908047499.

95 I. Haller, Elastic constants of the nematic liquid crystalline phase of p-methoxybenzylidene-p-n-butylaniline (MBBA), *J. Chem. Phys.*, 1972, **57**, 1400–1405, DOI: 10.1063/1.1678416.

96 M. Cvetinov, D. Obadović, M. Stojanović, D. Lazar, A. Vajda, N. Éber, K. Fodor-Csorba and I. Ristić, Mesophase behaviour of binary mixtures of bent-core and calamitic compounds, *Liq. Cryst.*, 2013, **40**, 1512–1519, DOI: 10.1080/02678292.2013.822938.

97 S. Parthasarathi, D. S. S. Rao, N. B. Palakurthy, C. V. Yelamaggad and S. Krishna Prasad, Binary System Exhibiting the Nematic to Twist-Bend Nematic Transition: Behavior of Permittivity and Elastic Constants, *J. Phys. Chem. B*, 2016, **120**, 5056–5062, DOI: 10.1021/acs.jpcb.6b03048.

98 N. Trbojevic, D. J. Read and M. Nagaraj, Dielectric properties of liquid crystalline dimer mixtures exhibiting the nematic and twist-bend nematic phases, *Phys. Rev. E*, 2017, **96**, 52703, DOI: 10.1103/PhysRevE.96.052703.

99 M. R. Tuchband, M. Shuai, K. A. Graber, D. Chen, L. Radzihovsky, A. Klittnick, L. Foley, A. Scarbrough, J. H. Porada, M. Moran, E. Korblova, D. M. Walba, M. A. Glaser, J. E. Maclennan and N. A. Clark, The twist-bend nematic phase of bent mesogenic dimer CB7CB and its mixtures, in APS March Meeting 2016, 2015.

100 B. Zhang and H. Kitzerow, Pattern Formation in a Nematic Liquid Crystal Mixture with Negative Anisotropy of the Electric Conductivity—A Long-Known System with "Inverse" Light Scattering Revisited, *J. Phys. Chem. B*, 2016, **120**, 6865–6871, DOI: 10.1021/acs.jpcb.6b05080.

101 B. Allen and R. Daniel Louis, Method for increasing the conductivity of electrically resistive organic materials, 1975, https://patents.google.com/patent/US4033905A/en.

102 Nissan Chemicals: Polyimide Data Sheet: Alignment Coatings for LCDs-SUNEVER Series-1.

103 I. S. Grant, S. Ian, W. R. Phillips and R. William, *Electromagnetism*, Wiley, 1975.

104 M. G. Clark, E. P. Raynes, R. A. Smith and R. J. A. Tough, Measurement of the permittivity of nematic liquid crystals in magnetic and electric fields using extrapolation procedures, *J. Phys. D: Appl. Phys.*, 1980, **13**, 2151–2164, DOI: 10.1088/0022-3727/13/11/025.

105 K. R. Welford and J. R. Sambles, Analysis of Electric Field Induced Deformations in a Nematic Liquid Crystal for any Applied Field, *Mol. Cryst. Liq. Cryst.*, 1987, **147**, 25–42, DOI: 10.1080/00268948708084622.

106 C. Meyer, G. R. Luckhurst and I. Dozov, The temperature dependence of the heliconical tilt angle in the twist-bend nematic phase of the odd dimer CB7CB, *J. Mater. Chem. C*, 2015, **3**, 318–328, DOI: 10.1039/C4TC01927J.

107 I. Haller, Thermodynamic and static properties of liquid crystals, *Prog. Solid State Chem.*, 1975, **10**, 103–118, DOI: 10.1016/0079-6786(75)90008-4.

108 J. C. Jones, Comparison of the P2 and P4 order parameters between symmetric and asymmetric liquid crystalline dimers with twist bend nematic phases. Special symposium: twist-bend nematics and beyond, University of Southampton, 2016, Unpublished.

109 G. R. Luckhurst, C. Zannoni, P. L. Nordio and U. Segre, A molecular field theory for uniaxial nematic liquid crystals formed by non-cylindrically symmetric molecules, *Mol. Phys.*, 1975, **30**, 1345–1358, DOI: 10.1080/00268977500102881.

110 B. Dressel and W. Pesch, Competition between electro-convection and Fréedericksz distortions in nematic liquid crystals with slightly positive dielectric anisotropy, *Phys. Rev. E: Stat., Nonlinear, Soft Matter Phys.*, 2003, **67**, 031707, DOI: 10.1103/PhysRevE.67.031707.

111 H. Wang, T. X. Wu, S. Gauza, J. R. Wu and S. Wu, A method to estimate the Leslie coefficients of liquid crystals based on MBBA data, *Liq. Cryst.*, 2006, **33**, 91–98, DOI: 10.1080/02678290500446111.

112 A. Varanytsia and L.-C. Chien, Giant Flexoelectro-optic Effect with Liquid Crystal Dimer CB7CB, *Sci. Rep.*, 2017, **7**, 41333, DOI: 10.1038/srep41333.

113 L. Kramer, E. Bodenschatz, W. Pesch, W. Thom and W. Zimmermann, Invited Lecture. New results on the electrohydrodynamic instability in nematics New results on the electrohydrodynamic instability in nematics, *Liq. Cryst.*, 1989, **5**, 699–715, DOI: 10.1080/02678298908045420.

114 N. V. Madhusudana and V. A. Raghunathan, Influence of flexoelectricity on electrohydrodynamic instabilities in nematics, *Liq. Cryst.*, 1989, **5**, 1789–1812, DOI: 10.1080/02678298908045689.

115 Y. Xiang, H. Z. Jing, Z. D. Zhang, W. J. Ye, M. Y. Xu, E. Wang, P. Salamon, N. Éber and Á. Buka, Tunable Optical Grating Based on the Flexoelectric Effect in a Bent-Core Nematic Liquid Crystal, *Phys. Rev. Appl.*, 2017, **7**, 064032, DOI: 10.1103/PhysRevApplied.7.064032.

116 P. Tadapatri, K. S. Krishnamurthy and W. Weissflog, Patterned flexoelectric instability in a bent-core nematic liquid crystal, *Soft Matter*, 2012, **8**, 1202–1214, DOI: 10.1039/c1sm06870a.

117 R. Balachandran, V. P. Panov, Y. P. Panarin, J. K. Vij, M. G. Tamba, G. H. Mehl and J. K. Song, Flexoelectric behavior of bimesogenic liquid crystals in the nematic phase-observation of a new self-assembly pattern at the twist-bend nematic and the nematic interface, *J. Mater. Chem. C*, 2014, **2**, 8179–8184, DOI: 10.1039/c4tc01043d.